# SHORT COMMUNICATIONS

MINERALOGICAL MAGAZINE, SPETEMBER 1990, VOL. 54, PP. 501—7

# Complex sector zonation in ankerite: geochemical controls on crystal morphology and intersector element partitioning

LATE-STAGE void-filling ankerite in dolomitized Dinantian limestones from Fife (Table 1, Fig. 1) displays well developed sector zonation (Fig. 2) which is sometimes combined with concentric zonation (Fig. 3). Sector boundaries are zigzag in 2D section (Figs 2, 3) reflecting a complex 3D topography created by the rapid expansion and contraction of competing sectors during growth. Crystals cut almost parallel to one of these complex sector boundaries display two patterns of zonation which are not immediately obvious as sector zonation: firstly, concentric zonation which appears to cross sector boundaries without change of orientation, and secondly, a comb pattern in which fingers of one composition are enclosed by a second composition (Fig. 4). The ankerite is consistently dominated by the $\{10\bar{1}4\}$ sectors with the minor sectors developed under $\{11\bar{2}0\}$ or very rarely $\{10\bar{1}1\}$ (Fig. 5). There is no correlation between changes in crystal morphology, as recorded by the contraction or expansion of sectors, and concentric growth zonation.

The ankerite is largely constrained to fractures and is believed to have precipitated from highly evolved diagenetic brines at temperatures of between 80 and 100°C (Searl and Fallick, 1990). It has a variable $^{13}C$ which indicates the importance of organic maturation in the fluid source rocks and, given the organic-rich nature of the Dinantian succession in Fife, it is probable that the precipitating fluid had a relatively high $pCO_2$. It is possible that precipitation was triggered by periodic reduction in formation fluid pressures through seismic activity (Searl and Fallick, 1990; Searl, in prep.).

## Chemistry of the sectors

The $\{10\bar{1}4\}$ sectors are consistently Fe-enriched, Mg-depleted, and usually slightly Ca and Mn-enriched, relative to the minor $\{11\bar{2}0\}$ sectors (Table 2). This contrasts with previous work on sector-zoned dolomites in which $\{11\bar{2}0\}$ sectors were found to be Mg and Fe-enriched relative to $\{10\bar{1}4\}$ sectors (Reeder and Prosky, 1986). Within individual growth sectors there is a tendency for Fe and Mn contents to show a positive co-variation and for Fe and Ca contents to show a negative co-variation.

## Controls on crystal morphology

Sector zonation is a consequence of the non-equivalence of surface cation sites on growing crystal faces and is preserved where crystal growth was faster than the rate of cation diffusion in the lattice (Namkamura, 1973). Lattice diffusion in carbonates is negligible at diagenetic temperatures (Barber and Riaz Khan, 1987) which suggests that sector zonation will occur in most carbonate crystals composed of two or more forms. The comparatively recent documentation of sector zonation in dolomites (Reeder and Prosky, 1986) and its apparent rarity is due to the tendency of dolomite to occur as simple rhombic crystals (only 2 of 20 recent articles in the Journal of Sedimentary Petrology, volumes 56–58, describe dolomite crystals with additional non-rhombic faces). The development of non-rhombic faces appears to be limited to some evaporative (Naiman *et al.*, 1983) and some poorly constrained burial (Banner *et al.*, 1988; Coniglio and James, 1988) settings.

Crystal morphology is dominated by the slowest growing faces and crystal habit in non-carbonate minerals precipitated from solution has been shown to be sensitive both to temperature (e.g. Murowchick and Barnes, 1987) and to small amounts of dissolved foreign species in solution (e.g. Cody and Cody, 1988). The Hartman-Perdok (1955) theory of crystal morphology predicts that trigonal carbonates should commonly crystal-

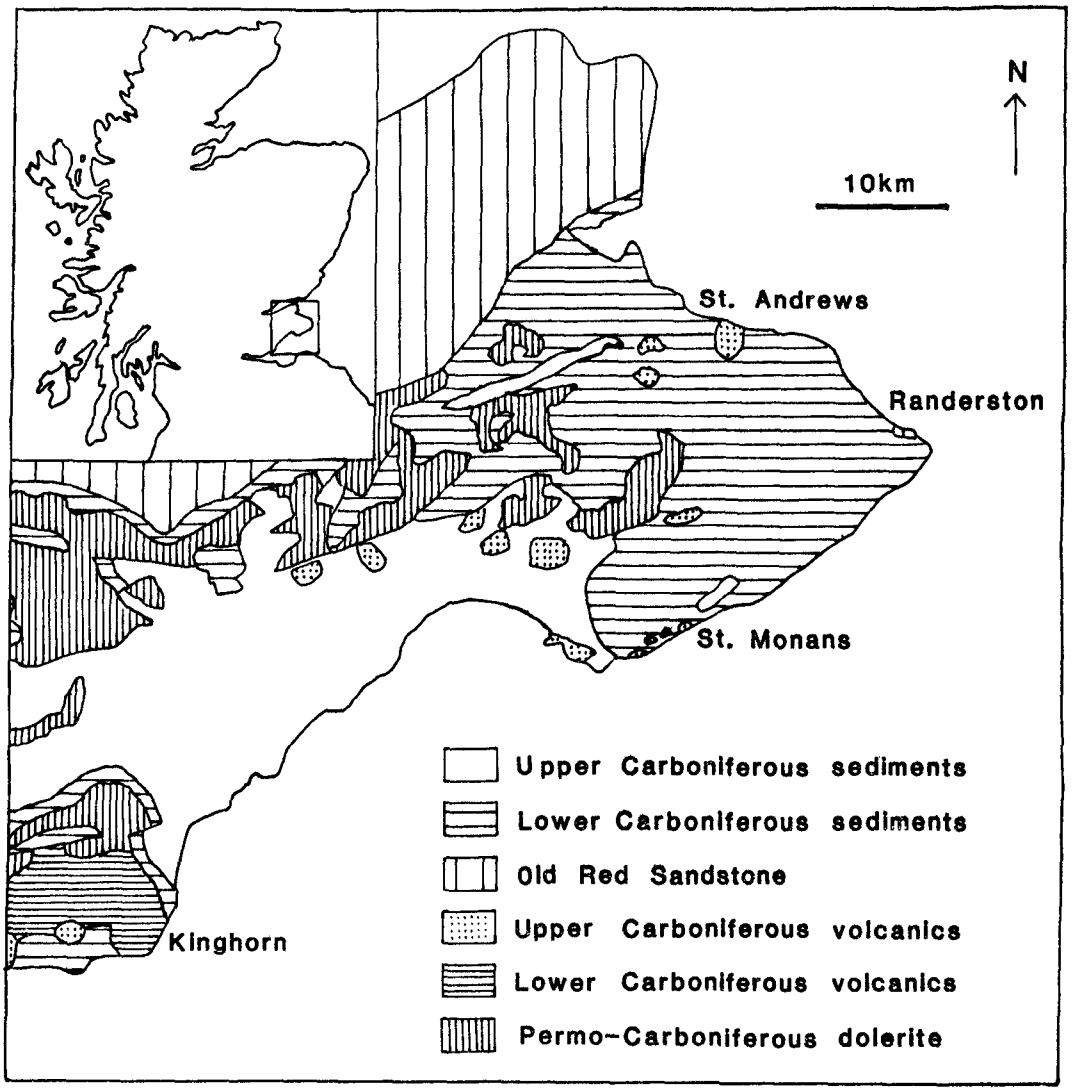


FIG. 1. Sample localities.

lize with $\{10\bar{1}4\}$ faces, but calcite develops a wide variety of other forms (Dickson, 1983). Calcite morphology has been related to fluid Ca/Mg ratios (Folk and Land, 1975), precipitation rates (Given and Wilkinson, 1985) and surface charge effects related to relative cation and $CO_3^{2-}$ availabilities (Given and Wilkinson, 1985; Lahann, 1978). The development of polyhedral dolomite in some evaporative settings may be due either to adsorption of foreign species on crystal faces or rapid growth rates. In most diagenetic environments, however, growth on the $\{10\bar{1}4\}$ faces of dolomite is severely retarded relative to other forms. The

Table 1: Sample Localities: all samples are from veins in Dinantian Limestones, Fife, Scotland.

| Sample Number | Locality | Grid Reference |
|---|---|---|
| BH7 | Boarhills | NO591144 |
| 88/8/5 | Randerston Limestone II | NO612117 |
| 88/5/5 | Randerston Limestone V | NO608116 |
| 88/6/3 | Randerston Limestone VI | NO609115 |
| 88/13/3 | Randerston Limestone VI | NO613114 |
| 88/20/2 | Randerston Limestone IX | NO616113 |
| KH42 | ) Kinniny Limestones | NT282890 |
| KH50 | ) ) Kinghorn | NT281886 |
| KH30 | 2nd Abden Limestone ) | NT278878 |
| LA13 | ) Lower Ardross Limestone, | NO520012 |
| LA22 | ) St. Monans | NO516012 |
| H7 | Mid Kinniny Limestone, St. Monans | NO530017 |

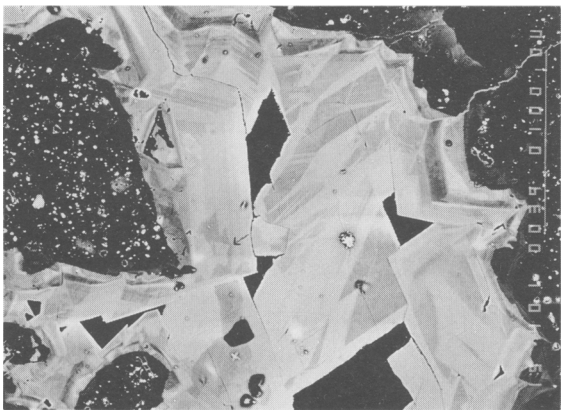

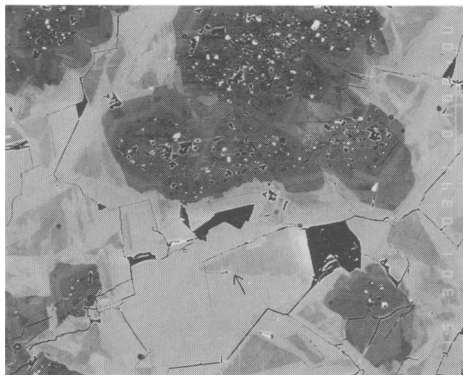

FIG. 2. (*left*). The central zone of a carbonate vein (KH42) in a backscattered scanning electron microscope (BSEM) image: the black speckled material is dolomite, the pale to mid gray phase ankerite, and the clean black areas void. The ankerite is both concentrically and sector zoned with zig-zag sector boundaries (see arrow).

FIG. 3. (*right*). BSEM image showing zig-zag competitive sector boundaries (arrow) in ankerite (pale to mid grey). Dark grey material is dolomite and black is void.

$\{10\bar{1}4\}$ faces differ from $\{11\bar{2}0\}$ and $\{10\bar{1}1\}$ faces in that lattice layers parallel to $\{10\bar{1}4\}$ are composed of equal numbers of cations and $CO_3^{2-}$, whereas lattice layers parallel to the other forms are alternately composed either entirely of cations or of $CO_3^{2-}$. If there is an excess of cations over $CO_3^{2-}$ in solution, or vice versa, $\{11\bar{2}0\}$ and $\{10\bar{1}1\}$ faces will develop a surface charge whereas $\{10\bar{1}4\}$ will remain electrostatically neutral. In most diagenetic fluids $CO_3^{2-}$ ions are much less readily available than metal cations and the $\{11\bar{2}0\}$ and $\{10\bar{1}1\}$ faces are likely to present an entirely cationic lattice layer to the solution. The small number of $CO_3^{2-}$ ions available will migrate preferentially to these charged faces causing such enhanced growth on these faces (see Lahann's 1978 model for calcite) that they are effectively not developed. In solutions with a relatively high availability of $CO_3^{2-}$ however, growth on these other faces will no longer be enhanced by electrostatic effects. In addition, in moderately to strongly alkaline fluids $OH^-$ is likely to become absorbed on exposed cationic lattice layers to a much greater extent than on mixed cation/anion layers. The presence of $OH^-$ strongly bound to surface cations will inhibit the initiation of new lattice layers and hence growth on $\{11\bar{2}0\}$ and $\{10\bar{1}1\}$ will be retarded relative to that on $\{10\bar{1}4\}$ in the presence of excess $OH^-$. In solutions with extremely high $CO_3^{2-}$ and relatively high pH therefore, growth on the non-rhombic faces is sufficiently retarded to allow development of non-rhombic forms and sector-zoned crystals. Such fluids with initially high $pCO_2$ (to generate high $[CO_3^{2-}]$) would be typical of deeply buried, organic-rich sediments, such as those believed to be the source of the fluids which precipitated the Fife ankerites.

In the Fife ankerites, changes in crystal morphology were independent of the cationic composition of the solution (Fig. 2) and the only other obvious parameter, which could vary rapidly and dramatically through time, is pore-fluid pressure and thus $pCO_2$. The zig-zag sector boundaries may, therefore, reflect oscillating fluid $pCO_2$ (Figs 6, 7) in response to the periodic release of fluid overpressures by fold movements during post-Carboniferous regional extension.

## Reassessment of the Reeder and Prosky (1986) model of sector zonation

Reeder and Prosky (1986) were able to partly explain inter-sector element partitioning by applying Dowty's (1976) model of crystal growth to dolomite. Their model, however, suggests all sector zoned dolomites should show similar patterns of inter-sector compositional variation which is inconsistent with the data presented here. The Reeder and Prosky model was largely conceived from the view-point of lattice geometry and with very little consideration of solution composition. Consequently a significant omission in their reasoning is consideration of the crystal/ligand field stabilization energy differences for Mn and Fe ions in surface sites on difference faces. Cations on surface sites will be partly co-ordinated

Table 2: Fife Ankerites: Electron Probe Data (mol%$MCO_3$)

| Sample Number | {1120} sector Ca | Mg | Fe | Mn | {1014} sector Ca | Mg | Fe | Mn |
|---|---|---|---|---|---|---|---|---|
| BH7 | 49.84 | 32.20 | 17.44 | 0.52 | 52.34 | 26.49 | 20.38 | 0.79 |
| | 50.06 | 33.12 | 16.38 | 0.45 | 51.94 | 25.59 | 21.52 | 0.95 |
| | 49.90 | 32.73 | 16.69 | 0.41 | 52.40 | 27.16 | 19.79 | 0.65 |
| | 50.32 | 32.82 | 16.37 | 0.48 | 50.73 | 26.81 | 20.81 | 0.64 |
| | 50.17 | 32.85 | 16.27 | 0.70 | 50.51 | 30.21 | 18.68 | 0.59 |
| 88/8/5 | 48.55 | 40.82 | 10.17 | 0.45 | 48.12 | 40.29 | 11.18 | 0.40 |
| | 47.00 | 36.29 | 17.26 | 0.45 | 47.69 | 33.58 | 18.19 | 0.55 |
| | 47.55 | 33.35 | 18.43 | 0.67 | 47.92 | 31.79 | 19.78 | 0.51 |
| 88/5/5 | 49.89 | 31.04 | 18.54 | 0.53 | 49.54 | 30.47 | 19.24 | 0.73 |
| | 49.93 | 26.63 | 18.27 | 0.60 | 50.07 | 31.20 | 20.36 | 0.51 |
| | 50.03 | 31.77 | 17.54 | 0.66 | 51.30 | 29.06 | 16.90 | 0.54 |
| 88/6/3 | 50.79 | 27.10 | 21.16 | 0.95 | 51.23 | 24.40 | 23.26 | 1.10 |
| | 50.47 | 32.76 | 16.34 | 0.44 | 51.01 | 26.48 | 21.67 | 0.83 |
| | 50.50 | 33.07 | 15.96 | 0.44 | 50.79 | 28.02 | 20.40 | 0.79 |
| 88/13/3 | 49.97 | 31.04 | 18.18 | 0.81 | 50.67 | 27.22 | 21.22 | 0.89 |
| 88/20/2 | 49.84 | 33.86 | 15.69 | 0.60 | 50.88 | 28.69 | 19.55 | 0.88 |
| | 49.54 | 33.94 | 16.07 | 0.44 | 50.99 | 27.39 | 20.42 | 1.20 |
| KH42 | 50.3 | 40.4 | 8.9 | 0.4 | 48.8 | 35.1 | 15.2 | 0.39 |
| | 49.3 | 38.1 | 12.0 | 0.6 | 49.1 | 32.7 | 17.0 | 1.2 |
| | 48.8 | 34.0 | 16.3 | 0.7 | 49.8 | 29.1 | 19.8 | 1.3 |
| | 48.8 | 34.8 | 15.5 | 0.9 | 49.5 | 30.4 | 19.1 | 1.9 |
| | | | | | 49.4 | 28.9 | 20.3 | 1.3 |
| | 50.0 | 36.0 | 13.3 | 0.7 | 49.8 | 46.1 | 4.0 | 0.1 |
| KH50 | 49.4 | 30.1 | 19.4 | 1.1 | 50.2 | 27.7 | 20.9 | 1.1 |
| | 49.5 | 39.0 | 11.0 | 0.5 | 49.6 | 37.2 | 12.6 | 0.6 |
| KH30 | 51.19 | 39.76 | 8.30 | 0.76 | 51.04 | 37.95 | 9.54 | 1.46 |
| | 49.53 | 41.43 | 8.20 | 0.84 | 50.15 | 39.25 | 9.29 | 1.31 |
| | 48.79 | 41.30 | 9.02 | 0.87 | 51.61 | 35.95 | 11.36 | 1.09 |
| | 50.30 | 39.37 | 9.23 | 1.11 | 50.72 | 37.09 | 11.00 | 1.20 |
| | 50.92 | 47.46 | 1.37 | 0.24 | 50.09 | 37.76 | 10.85 | 1.31 |
| | 51.18 | 46.98 | 1.52 | 0.33 | 50.54 | 37.86 | 10.33 | 1.28 |
| | 51.3 | 47.16 | 1.31 | 0.23 | 50.71 | 39.37 | 8.93 | 0.99 |
| | 50.85 | 47.56 | 1.35 | 0.25 | 50.78 | 36.81 | 11.23 | 1.17 |
| | 50.76 | 47.54 | 1.42 | 0.07 | | | | |
| | 50.80 | 47.60 | 1.24 | 0.36 | | | | |
| | 50.64 | 47.61 | 1.19 | 0.36 | | | | |
| LA13 | 49.08 | 34.02 | 16.28 | 0.62 | 49.94 | 29.32 | 19.69 | 1.05 |
| | 49.39 | 34.76 | 15.16 | 0.70 | 50.60 | 29.12 | 19.29 | 0.98 |
| | | | | | 50.71 | 28.88 | 19.95 | 0.88 |
| | | | | | 49.96 | 29.47 | 19.56 | 1.01 |
| | 50.10 | 38.94 | 10.39 | 0.58 | 50.34 | 32.12 | 16.88 | 0.67 |
| | 53.00 | 38.13 | 5.86 | 3.00 | 53.64 | 37.32 | 5.87 | 3.17 |
| | 52.21 | 34.39 | 12.90 | 0.49 | 52.60 | 32.27 | 14.54 | 0.58 |
| | | | | | 52.76 | 31.97 | 14.87 | 0.4 |
| LA22 | 50.01 | 33.15 | 16.23 | 0.61 | 49.50 | 30.81 | 18.85 | 0.89 |
| | 49.62 | 32.82 | 16.63 | 0.72 | 51.54 | 28.21 | 19.38 | 0.87 |
| | | | | | 51.70 | 29.08 | 18.26 | 0.96 |
| | 50.91 | 28.30 | 19.72 | 1.08 | 50.27 | 26.51 | 21.92 | 1.30 |
| H7 | 49.3 | 38.4 | 11.6 | 0.6 | 49.7 | 36.5 | 13.3 | 0.5 |
| | 49.0 | 34.1 | 16.3 | 0.5 | 49.3 | 32.0 | 18.0 | 0.7 |
| | 49.4 | 37.8 | 12.5 | 0.4 | 49.9 | 31.2 | 18.0 | 0.9 |
| | 49.0 | 38.1 | 12.6 | 0.3 | | | | |
| | 49.2 | 37.6 | 12.9 | 0.3 | 49.2 | 35.7 | 14.6 | 0.4 |
| | 49.2 | 30.1 | 19.9 | 0.8 | 50.1 | 28.2 | 20.8 | 0.8 |
| | 51.1 | 33.8 | 14.6 | 0.6 | 49.4 | 33.0 | 17.9 | 0.7 |
| | 49.0 | 38.7 | 11.9 | 0.4 | 49.1 | 31.9 | 18.3 | 0.7 |
| | 49.3 | 38.5 | 11.8 | 0.5 | 49.7 | 31.6 | 18.1 | 0.6 |
| | 49.8 | 39.2 | 10.7 | 0.4 | 49.2 | 32.9 | 17.1 | 0.7 |

Overall mean composition of ankerite: 50.7mol%$CaCO_3$ (s.d. = 0.18), 33.5mol%$MgCO_3$ (s.d. = 0.43), 14.7mol%$FeCO_3$ (s.d. = 0.52), 0.8mol%$MnCO_3$ (s.d. = 0.04).

Mean differences between sectors ({1014} - {1120}): +0.52mol%$CaCO_3$ (s.d. = 0.13), -3.99mol%$MgCO_3$ (s.d. = 0.7), +3.23mol%$FeCO_3$ (s.d. = 0.34), +0.24mol% $MnCO_3$ (s.d. = 0.09).

Analyses and BSEM imaging performed using a Jeol Superprobe 733 operated at 15kV and 15nA. Use of noncarbonate standards limits data comparability with other studies.

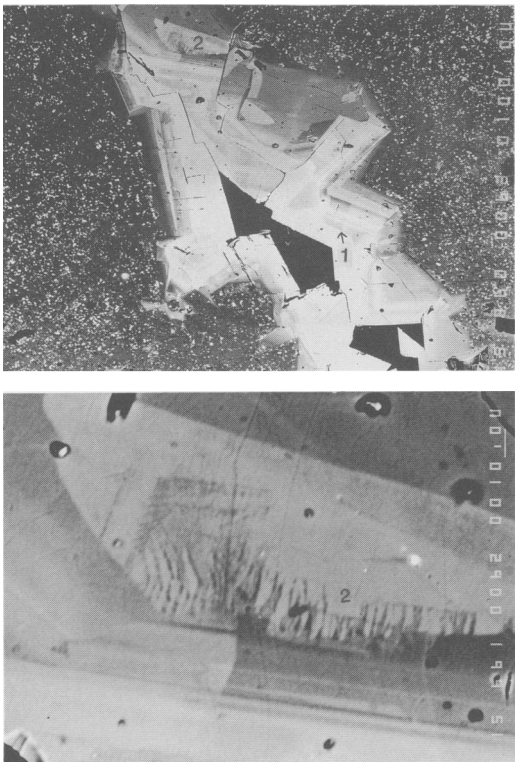

FIG. 4. Apparently anomalous patterns of compositional zonation which appear when a thin section is cut almost parallel to growth sector boundaries, intersecting the complex topography of these surfaces. Firstly, concentric growth zones show no change in orientation at the sector boundary, so that the crystal appears to have changed composition mid-face during growth (1). Secondly a comb pattern (2) appears to preserve a dendritic growth front, or a phase of etching between successive growth zones: however the angular change in orientation of 'dendrites' indicates that this a section through a zig-zag sector boundary. (BSEM, H7)

FIG. 5. Sector zoned ankerite (pale-mid grey) with minor development of Fe-enriched (pale grey) $\{10\bar{1}1\}$ sectors (arrow in $\{10\bar{1}4\}$ dominated crystals. There are also minor $\{11\bar{2}0\}$ sectors which are a darker grey than the surrounding material. (BSEM, 88/8/5)

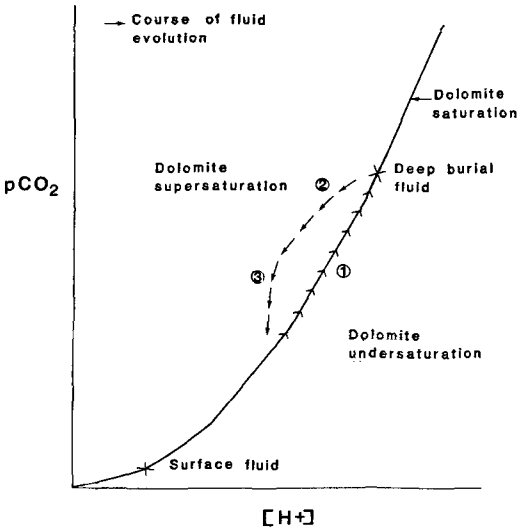


FIG. 6. Variation of fluid composition within a fracture which has periodic open communication with the surface (i.e. during fault movement): (1) gradual build-up of $pCO_2$ due to the maturation of organic matter in surrounding sediment, pH buffered by carbonate minerals; (2) fluid released along fault planes, reduction in $pCO_2$, pH adjusts to new equilibria with dissolved $CO_2$, generation of dolomite supersaturation; (3) precipitation of dolomite until equilibrium re-attained and the $pCO_2$ starts to build up prior to the next seismic event.

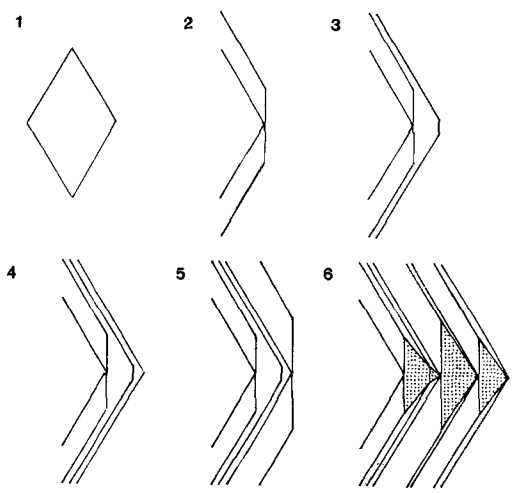


FIG. 7. Generation of competitive sector boundaries: (1) High $pCO_2$, high $[H^+]$, dolomite in equilibrium with surrounding fluid, simple rhombic morphology; (2) Sudden reduction in $pCO_2$, generation of high $[CO_3^{2-}]$ rapid growth on $\{10\bar{1}4\}$ and consequent development of $\{11\bar{2}0\}$; (3) continued dolomite precipitation, falling $[CO_3^{2-}]$ which causes retardation of growth on $\{10\bar{1}4\}$ such that crystal morphology is dominated by $\{10\bar{1}4\}$; (4) extreme retardation of growth on $\{10\bar{1}4\}$ crystal reverts to rhombic morphology, growth halted as $pCO_2$ begins to build up again; (5) as (2); (6) Continued oscillation in $pCO_2$ and therefore $[CO_3^{2-}]$ levels gives rise to highly competitive sector boundaries.

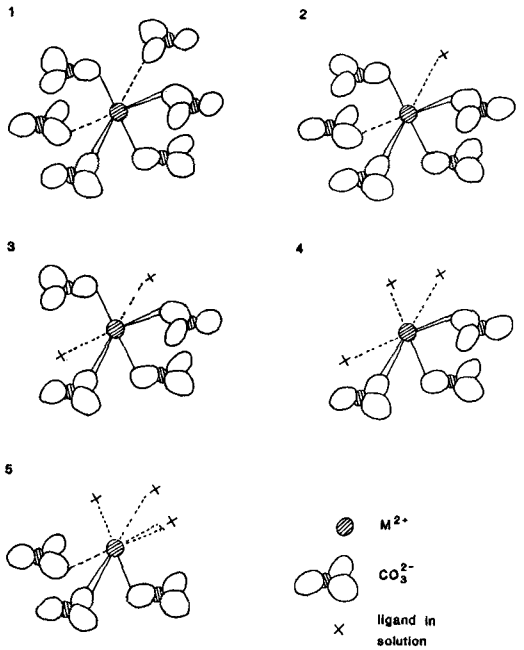


FIG. 8. Co-ordination of $M^{2+}$ in dolomite: comparison of lattice and surface sites. (1) octahedral co-ordination of $M^{2+}$ within the crystal; (2) $M^{2+}$ site on $\{10\bar{1}4\}$ faces; (3) $M^{2+}$ site on $\{11\bar{2}0\}$ faces; (4) $M^{2+}$ site on $\{10\bar{1}1\}$ faces; (5) $M^{2+}$ site on $\{0001\}$ faces.

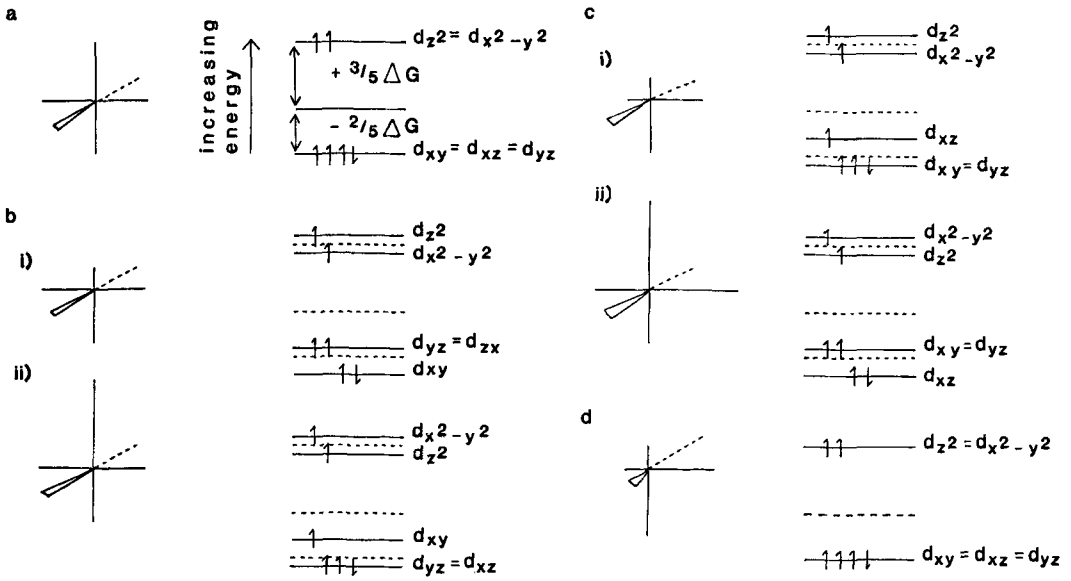


FIG. 9. *d* electron configurations for $Fe^{2+}$ (low spin): (*a*) Undistorted octahedron in which all ligands are of equal strength, $d_{x^2-y^2}$ and $d_{z^2}$ are degenerate with elevated energies, and $d_{xy}$, $d_{xz}$ and $d_{zy}$ are degenerate with lowered energies. The single orbital containing paired electrons is one of $d_{xy}$, $d_{xz}$, or $d_{zy}$, with an overall CFSE of −2/5 G. (*b*) Distortion of the octahedron along one axis by introduction of a single 'foreign' ligand [see Fig. 8(2)]: (i) introduction of a stronger ligand increases energies along one axis (ii) introduction of a weaker ligand decreases energies along one axis; in both cases the paired elctrons occupy the lowest, or one of the lower energy orbitals with a consequent gain in CFSE over the undistorted state. This gain in CFSE is greater when the foreign ligand is stronger, than the lattice ligands, leading to a single lowest energy orbital. (*c*) Distortion along two axes, assuming both foreign ligands to be equal [Fig. 8(3)]: (i) introduction of two stronger ligands (ii) introduction of two weaker ligands; the greatest gain in CFSE is when solution ligands are weaker than lattice ligands. (*d*) Distortion of octahedron along 3 axes [Fig. 8 (4 and 5)] produces degeneracy as in (*a*).

to lattice $CO_3^{2-}$ and partly to water molecules or other ligands in solution. The resultant distorted octahedral sites will show variable patterns of *d* orbital splitting (the Jahn-Teller effect), depending on surface site geometry and particularly on the ratio of lattice to solution coordination bonds (Fig. 8). The relative 'strength' of solution ligands versus lattice $CO_3^{2-}$ determines whether there is a greater CFSE/LFSE advantage associated with $\{10\bar{1}4\}$ cation sites in which the coordination octahedron is distorted along a single axis or with $\{11\bar{2}0\}$ sites in which the octahedron is distorted along two axes (Fig. 9). These CFSE/LFSE effects are not generally relevant to $Mn^{2+}$ in which electrons are usually evenly distributed through all five *d* orbitals, unless ligands are of sufficient strength to stabilize spin-paired electronic configurations. If the fluid does contain high ligand field strength species such as carbonyl groups or cyanide, then Fe or Mn in a surface site with a high degree of co-ordination to fluid ligands might adapt spin-paired electronic configurations with a CFSE advantage over low spin configurations on other faces. Although CFSE/LFSE is unlikely to be the cause of sector zonation, some of the variability in patterns of element partitioning may be due to CFSE/LFSE effects associated with the availabilities of different ligands in solution. This suggests the future possibility of using patterns of intersector element variation to partly constrain fluid compositions.

**Acknowledgements**

I thank the Geology Department of St Andrews University for use of their electron microprobe, with particular thanks to Donald Herd and Ed Stephens for their help. I also thank Colin Donaldson, Ian Fairchild and Jim Hendry for useful discussion.

**References**

Banner, J. L., Hanson, G. N. and Meyers, W. J. (1988) *J. Sed. Petrol.* **58,** 673–87.
Barber, D. J. and Riaz Khan, M. (1987) *Mineral. Mag.* **51,** 71–86.
Cody, R. D. and Cody, A. M. (1988) *J. Sed. Petrol.* **58,** 247–55.
Coniglio, M. and James, N. P. (1988) Ibid., 1032–45.
Dickson, J. A. D. (1983) *Phil. Trans. Roy. Soc. London*, **A309,** 465–502.
Dowty, E. (1976) *Am. Mineral.* **61,** 460–9.
Folk, R. L. and Land, L. S. (1975) *Am. Assoc. Petrol. Geol. Bull.* **59,** 60–8.
Given, R. K. and Wilkinson, B. H. (1985) *J. Sed. Petrol.* **55,** 109–19.
Hartman, P. and Perdok, W. G. (1955) *Acta Crystallogr.* **8,** 49–52.
Lahann, R. W. (1978) *J. Sed. Petrol.* **48,** 337–44.
Murowchick, J. B. and Barnes, H. L. (1987) *Am. Mineral.* **72,** 1241–50.
Naiman, E. R., Bein, A. and Folk, R. L. (1983) *J. Sed. Petrol.* **53,** 549–55.
Nakumura, Y. (1973) *Am. Mineral.* **58,** 986–90.
Reeder, R. J. and Prosky, J. L. (1986) *J. Sed. Petrol.* **56,** 237–47.
Searl, A. and Fallick, A. E. (1990) *J. Geol. Soc. Lond.* (in press)

*[Manuscript received 11 September 1989; revised 18 January 1990]*



KEYWORDS: ankerite, sector zonation, carbonate crystal morphology.

*School of Earth Sciences, University of Birmingham, Birmingham, B15 2TT*

ALISON SEARL